Application of load-dependent Ritz vectors to probabilistic damage detection

Hoon Sohn[a] and Kincho H. Law[b]

Department of Civil and Environmental Engineering
Stanford University, Stanford, CA 94305, U.S.A.

ABSTRACT

This paper demonstrates the possibility of incorporating load-dependent Ritz vectors, as an alternative to modal parameters, into a Bayesian probabilistic framework for detecting damages in a structure. Recent research has shown that it is possible to extract load-dependent Ritz vectors from vibration tests. This paper shows that load-dependent Ritz vectors have the following potential advantages for damage detection over modal vectors: (1) In general, load-dependent Ritz vectors are more sensitive to damage than the corresponding modal vectors, and (2) substructures of interest can be made more observable using the load-dependent Ritz vectors generated from particular load patterns. An eight-bay truss structure and a five-story frame example are presented to illustrate the applicability of the proposed approach.

Keywords: Load-dependent Ritz vector, Bayesian probabilistic approach, damage detection

1. INTRODUCTION

Damage detection and heath monitoring of large scale structures are becoming an important challenge to engineering research. One common approach for global damage detection is to employ the vibration characteristics of a structure such as frequencies, modal vectors, and modal damping to predict the damage locations and to estimate the amount of damage. However, it has been shown that changes in the modal parameters might not be apparent at an early stage of damage. Also, the uncertainties caused by measurement noise, modeling error involved in an analytical model, and environmental changes such as variations in temperature and load conditions can impede the reliable identification of damage. Therefore, for reliable damage detection, the damage would need to cause significant changes in the modal parameters that are beyond the natural variability caused by the effects other than the damage.

Recent research has shown that it is possible to extract Ritz vectors from vibration tests.[1] The first Ritz vector is the static deformation of a structure due to a particular load applied to the structure. The subsequent vectors account for the inertial effects of the loading and are generated by iterative matrix multiplication and orthogonalization. Ritz vectors (or Lanczos vectors) have been shown very effective for dynamic and earthquake analyses, eigenvalue problems and model reductions. In this paper, we demonstrate the possibility of incorporating load-dependent Ritz vectors, as an alternative to modal parameters, into the previously proposed Bayesian probabilistic framework for damage detection.[2] This study is motivated by the following potential advantages of Ritz vectors over modal vectors: (1) In general, Ritz vectors are more sensitive to damage than the corresponding modal vectors, (2) substructures of interest can be made more observable using the Ritz vectors generated from particular load patterns, (3) the computation of Ritz vectors is less expensive than that of modal vectors (eigenvectors) and (4) while the practical difficulties of modal testing impede the extraction of a large number of meaningful modes, a larger number of Ritz vectors can be extracted by imposing different load patterns on a structure.

This paper is organized as follows: The next section reviews the theoretical formulation of the previously proposed Bayesian probabilistic approach.[2] Section 3 presents numerical examples to illustrate the effectiveness of the proposed method. Section 4 summarizes this paper.

Correspondence to Hoon Sohn
[a] Ph.D. candidate: E-mail: sohnhoon@leland.stanford.edu
[b] Professor: E-mail: law@ce.stanford.edu

2. THEORETICAL FORMULATION

Bayesian probabilistic approaches, which use modal parameters, have been applied to damage detection by researchers.[3,2] The idea is to search for the most probable damage event by comparing the relative probabilities for different damage scenarios, where the relative probability of a damage event is expressed in terms of the posterior probability of the damage event, given the estimated modal data sets from a structure. In this paper, the formulation of the relative posterior probability is based on an output error, which is defined as the difference between the estimated Ritz vectors and the theoretical Ritz vectors from the analytical model.

2.1. Notations and Assumptions

For an analytical model of a structure, we represent the system stiffness matrix $\mathbf{K}$ as an assembly of substructure stiffness matrices. For a model with N_{sub} substructures, the overall stiffness matrix can be expressed as:

$$\mathbf{K}(\Theta) = \sum_{i=1}^{N_{sub}} \theta_i \mathbf{K}_{si} \tag{1}$$

where $\mathbf{K}_{si}$ is the stiffness matrix of the ith substructure and θ_i $(0 \leq \theta_i \leq 1)$ is a nondimensional parameter which represents the contribution of the ith substructure stiffness to the system stiffness matrix. The nondimensional parameter θ_i is introduced to allow the modeling of damage in the ith substructure. A substructure is defined as *damaged* when the θ value is less than a specified threshold. As damage locations and amount are determined according to the θ values, the system stiffness matrix in Equation (1) is expressed as a function of $\Theta = \{\theta_i; i = 1, ..., N_{sub}\}$.

Test data sets are assumed to be collected from repeated vibration tests. When vibration tests are repeated N_s times, the total collection of N_s data sets is denoted as:

$$\hat{\Psi}_{N_s} = \{\hat{\psi}(n) \ : \ n = 1, ..., N_s\} \tag{2}$$

A data set $\hat{\psi}(n)$ in Equation (2) is composed of Ritz vectors estimated from the nth vibration test:

$$\hat{\psi}(n) = \left[\hat{\mathbf{r}}_1^{nT}, ..., \hat{\mathbf{r}}_{N_r}^{nT}\right]^T \in \mathbf{R}^{N_t} \tag{3}$$

where $\hat{\mathbf{r}}_i^n$ denotes the ith estimated Ritz vector in the nth data set. The Ritz vector $\hat{\mathbf{r}}_i^n$ $(\hat{\mathbf{r}}_i^n \in \mathbf{R}^{N_d})$ has components corresponding to the instrumented degrees of freedom (DOFs). The variables N_t, N_d and N_r represent the total number of components in a data set $\hat{\psi}(n)$, the number of the measured DOFs and the number of the estimated Ritz vectors, respectively.

Let H_j denote a hypothesis for a damage event which can contain any number of substructures as damaged, and the initial degree of belief about the hypothesis H_j is represented with a prior probability $P(H_j)$. Using Baye's theorem, the posterior probability $P(H_j|\hat{\Psi}_{N_s})$, after observing the estimated data sets $\hat{\Psi}_{N_s}$, is given as:

$$P(H_j|\hat{\Psi}_{N_s}) = \frac{P(\hat{\Psi}_{N_s}|H_j)}{P(\hat{\Psi}_{N_s})} P(H_j) \tag{4}$$

The most likely damaged substructures are the ones included in the hypothesis H_{max} which has the largest posterior probability, i.e.

$$P(H_{max}|\hat{\Psi}_{N_s}) = \max_{\forall H_j} P(H_j|\hat{\Psi}_{N_s}) \tag{5}$$

Since the objective is to determine the most probable damage hypothesis (event), only the relative posterior probabilities of alternative hypotheses are of interest. We attempt to avoid the explicit expression of a posterior probability $P(H_j|\hat{\Psi}_{N_s})$ since the precise calculation of $P(\hat{\Psi}_{N_s}|H_j)$ is a difficult task. To overcome these difficulties, we focus on the relative comparisons of posterior probabilities.

2.2. Determination of the Most Probable Damage Event

When applying Equation (4) to calculate the posterior probability $P(H_j|\hat{\Psi}_{N_s})$, the only undefined term is $P(\hat{\Psi}_{N_s}|H_j)$. The prior probability of a hypothesis $P(H_j)$ is the prior information given by users and the probability of estimated test data $P(\hat{\Psi}_{N_s})$ is simply a normalizing constant.

As shown in Equation (1), less than a unity value for θ_i reflects the stiffness decrease in the ith substructure. As noted earlier, damage is characterized by stiffness reduction. When θ_i is less than a specified threshold $\theta_i^*(<1)$, the ith substructure is defined as *damaged*. If we define $\Theta_{H_j}^1$ as a set of θ_i's corresponding to the damaged substructures in a hypothesis H_j and $\Theta_{H_j}^2$ as the remaining θ_i's, the conditional probability $P(\hat{\Psi}_{N_s}|H_j)$ can be interpreted as the probability of obtaining $\hat{\Psi}_{N_s}$ when the θ_i's in $\Theta_{H_j}^1$ are less than or equal to their threshold θ_i^*'s and the remaining θ_i's stay within $\theta_i^* < \theta_i \leq 1$. Denoting $\Omega_{H_j}^*$ as the range of Θ_{H_j} such that $0 \leq \Theta_{H_j}^1 \leq \Theta_{H_j}^{1,*}$ and $\Theta_{H_j}^{2,*} < \Theta_{H_j}^2 \leq 1$, the conditional probability $P(\hat{\Psi}_{H_j}|H_j)$ becomes:

$$P(\hat{\Psi}_{N_s}|H_j) = P(\hat{\Psi}_{N_s}|\Theta_{H_j} < \Omega_{H_j}^*) = \frac{P(\Theta_{H_j} < \Omega_{H_j}^*|\hat{\Psi}_{N_s})\ P(\hat{\Psi}_{N_s})}{P(\Theta_{H_j} < \Omega_{H_j}^*)}$$
$$= \frac{P(\hat{\Psi}_{N_s})}{P(\Theta_{H_j} < \Omega_{H_j}^*)} \int_{\Theta_{H_j} < \Omega_{H_j}^*} f(\Theta_{H_j}|\hat{\Psi}_{N_s}) d\Theta_{H_j} \tag{6}$$

where $\Theta_{H_j}^{1,*}$ and $\Theta_{H_j}^{2,*}$ are the sets of damage thresholds for $\Theta_{H_j}^1$ and $\Theta_{H_j}^2$, respectively, and $f(\Theta_{H_j}|\hat{\Psi}_{N_s})$ is a conditional probability density function (PDF) of Θ_{H_j} given $\hat{\Psi}_{N_s}$. Furthermore, $\Theta_{H_j} < \Omega_{H_j}^*$ indicates that Θ_{H_j} are within the range of $\Omega_{H_j}^*$ such that $0 \leq \Theta_{H_j}^1 \leq \Theta_{H_j}^{1,*}$ and $\Theta_{H_j}^{2,*} < \Theta_{H_j}^2 \leq 1$.

If we define the most probable parameter values $\Theta_{H_j}^{max}$, given a hypothesis H_j, such that:

$$f(\Theta_{H_j}^{max}|\hat{\Psi}_{N_s}) = \max_{\Theta_{H_j} < \Omega_{H_j}^*} f(\Theta_{H_j}|\hat{\Psi}_{N_s}) \tag{7}$$

then the upper bound of $P(\hat{\Psi}_{N_s}|H_j)$ in Equation (6) becomes:

$$P_U(\hat{\Psi}_{N_s}|H_j) = \frac{P(\hat{\Psi}_{N_s})}{P(\Theta_{H_j} < \Omega_{H_j}^*)} \int_{\Theta_{H_j} < \Omega_{H_j}^*} f(\Theta_{H_j}^{max}|\hat{\Psi}_{N_s}) d\Theta_{H_j} \tag{8}$$
$$= \frac{P(\hat{\Psi}_{N_s})}{P(\Theta_{H_j} < \Omega_{H_j}^*)}\ f(\Theta_{H_j}^{max}|\hat{\Psi}_{N_s}) \int_{\Theta_{H_j} < \Omega_{H_j}^*} 1\ d\Theta_{H_j}$$

For simplification, we assume that if damage occurs, it can have any arbitrary amount with equal probability. That is, we assign a uniform probability density function to θ_i such that:

$$f(\theta_i) = \begin{cases} 1 & \text{if } 0 \leq \theta_i \leq 1 \\ 0 & \text{otherwise} \end{cases} \tag{9}$$

Furthermore, if θ_i's are assumed to be independent, the following two equations hold:

$$f(\Theta_{H_j}) = \prod_{\forall\ \theta_i \in \Theta_{H_j}} f(\theta_i) = 1 \tag{10}$$

$$\frac{1}{P(\Theta_{H_j} < \Omega_{H_j}^*)} = \frac{1}{\int_{\Theta_{H_j} < \Omega_{H_j}^*} f(\Theta_{H_j}) d\Theta_{H_j}} = \frac{1}{\int_{\Theta_{H_j} < \Omega_{H_j}^*} 1\ d\Theta_{H_j}} \tag{11}$$

Substituting Equation (11) into Equation (8), $P_U(\hat{\Psi}_{N_s}|H_j)$ can be simplified as:

$$P_U(\hat{\Psi}_{N_s}|H_j) = f(\Theta_{H_j}^{max}|\hat{\Psi}_{N_s})\ P(\hat{\Psi}_{N_s}) \tag{12}$$

The next step is to compute the conditional PDF, $f(\Theta_{H_j}^{max}|\hat{\Psi}_{N_s})$. First, let's define an output error $e(n, \Theta_{H_j})$ as:

$$e(n, \Theta_{H_j}) = \hat{\psi}(n) - \psi(\Theta_{H_j});\ n = 1, ..., N_s \tag{13}$$

where $\hat{\psi}(n)$ is defined in Equation (3). Given Θ_{H_j}, an analytical data set $\psi(\Theta_{H_j})$ is defined similar to Equation (3):

$$\psi(\Theta_{H_j}) = \left[\mathbf{r}_1^T(\Theta_{H_j}), ..., \mathbf{r}_{N_r}^T(\Theta_{H_j})\right]^T \in \mathbf{R}^{N_t} \tag{14}$$

It should be noted that a Ritz vector $\mathbf{r}_i(\Theta_{H_j})$ in Equation (14) has only the components associated with the measured DOFs.

Assuming each component of the output error $\{e_i(n, \Theta_{H_j}); n = 1, ..., N_s\}$ to be a multivariate normal distribution with zero mean and variance σ_i, the conditional joint PDF of Θ_{H_j} becomes:

$$f(\Theta_{H_j}|\hat{\Psi}_{N_s}) = f(e(n, \Theta_{H_j})|\hat{\Psi}_{N_s}) = k \cdot exp\{ - J(\hat{\Psi}_{N_s}, \Theta_{H_j})\} \tag{15}$$

where $k = \frac{1}{[2\pi]^{\frac{N_s}{2}}} \frac{1}{\|\mathbf{C}_{\hat{\Psi}}\|^{\frac{1}{2}}}$, $\|\mathbf{C}_{\hat{\Psi}}\| = det|diag[\sigma_1^2, ..., \sigma_{N_t}^2]| = \prod_{i=1}^{N_t} \sigma_i^2$, and the variance σ_i can be evaluated from observations of the estimated Ritz vector sets. When a large number of experimental data sets are available, sample standard deviations (or variances) can be extracted from the data sets. When modal data sets available are not sufficient to estimate the variances, we assign uniform coefficient of variance (COV) to all components of $e(n, \Theta_{H_j})$. Furthermore, the error function $J(\hat{\Psi}_{N_s}, \Theta_{H_j})$ is:

$$J(\hat{\Psi}_{N_s}, \Theta_{H_j}) = \frac{1}{2} \sum_{n=1}^{N_s} \left[\hat{\psi}(n) - \psi(\Theta_{H_j})\right]^T \mathbf{C}_{\hat{\Psi}}^{-1} \left[\hat{\psi}(n) - \psi(\Theta_{H_j})\right] \tag{16}$$

From Equations (4), (12) and (15), the upper bound of $P(H_j|\hat{\Psi}_{N_s})$ becomes:

$$P_U(H_j|\hat{\Psi}_{N_s}) = f(\Theta_{H_j}^{max}|\hat{\Psi}_{N_s})P(H_j) = exp\{ - J(\hat{\Psi}_{N_s}, \Theta_{H_j}^{max})\} \cdot P(H_j) \cdot k \tag{17}$$

From Equation (17) and the fact that the relative comparison of $P_U(H_j|\hat{\Psi}_{N_s})$ is independent of the constant k, the following relationships hold:

$$\begin{aligned} \max\left[P_U(H_i|\hat{\Psi}_{N_s}), P_U(H_j|\hat{\Psi}_{N_s})\right] &= \max\left[ln\, P_U(H_i|\hat{\Psi}_{N_s}), ln\, P_U(H_j|\hat{\Psi}_{N_s})\right] = \\ \min\left[J(\hat{\Psi}_{N_s}, \Theta_{H_i}^{max}) - lnP(H_i), J(\hat{\Psi}_{N_s}, \Theta_{H_j}^{max}) - lnP(H_j)\right] & \end{aligned} \tag{18}$$

where ln denotes a natural logarithm. Therefore, the most probable hypothesis H_{max} in Equation (5) satisfies:

$$J(\hat{\Psi}_{N_s}, \Theta_{H_{max}}^{max}) - lnP(H_{max}) = \min_{\forall H_j}\left[J(\hat{\Psi}_{N_s}, \Theta_{H_j}^{max}) - lnP(H_j)\right] \tag{19}$$

Now, the comparison of posterior probabilities can be conducted by examining only the error function $J(\hat{\Psi}_{N_s}, \Theta_{H_j}^{max})$ and the prior probability $P(H_j)$.

A branch-and-bound search scheme is proposed to expedite the search for the most likely damaged substructure without exhaustively examining all the possible damage cases. Furthermore, sensitivities of Ritz vectors with respect to the stiffness change of a member is derived to measure the relative significance of the Ritz vectors to damages and a weighting scheme of Ritz vectors is proposed based on the derived sensitivity. For a detailed explanation of the branch-and-bound scheme and the sensitivity analyses, readers are referred to References 2 and 4.

3. NUMERICAL EXAMPLES

This section demonstrates the potential applicability of Ritz vectors to damage detection of structures and the better sensitivity of Ritz vectors over modal vectors. A three-dimensional truss structure and a five-story frame building structure are employed for numerical examples. The first example structure is an eight-bay truss structure from the NASA dynamic scale model technology (DSMT) program of Langley Research Center. A detailed description of the example structure can be found in Reference 5. The second example structure is a five-story frame building. This section is organized as follows: First, sensitivity analyses of Ritz vectors are conducted and the sensitivities of Ritz vectors are compared to those of modal vectors. Second, the damage detection of the eight-bay truss structure is conducted by changing damage locations and load patterns. Furthermore, the damage detection using Ritz vectors is compared to the damage detection using modal parameters. Third, the proposed method is applied to the damage detection of the five-story frame building.

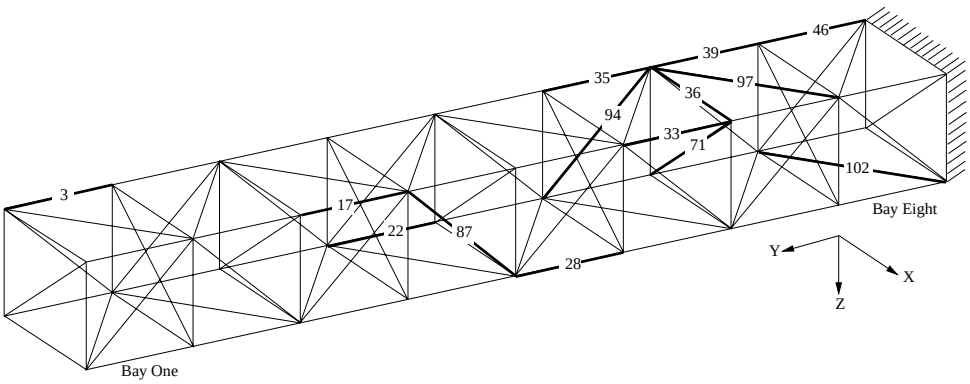

Figure 1. An Eight-Bay Truss Structure

3.1. Sensitivity Analyses of Ritz Vectors

In this subsection, an eight-bay truss structure is employed for the sensitivity analyses. The structure is an eight-bay truss structure fixed at one end, as shown in Figure 1. The structure is modeled using 104 truss elements, 36 nodes and 96 DOFs. Five truss members at the fixed end are not included in the model. Furthermore, each truss member is assigned as a substructure. Figure 2 shows the classification of the truss members into four different lacing patterns: longeron, batten, face diagonal and side diagonal. Load pattern 1 shown in Figure 3 (a) is employed for the generation of Ritz vectors.

The sensitivity analysis is conducted by comparing the changes of the Ritz and modal vectors as the stiffness of each substructure (member) deteriorates. Selected results from the comparisons are presented in Figures 4, 5 and 6. Figure 4 (a) shows how the first five Ritz vectors change as the stiffness loss of the 33th member (a longeron in bay six) varies from 0% to 100%. For a simple graphical representation, the ratio of $\|\mathbf{r}_r^h - \mathbf{r}_r^d\|^2$ to $\|\mathbf{r}_r^h\|^2$ is computed to indicate the change of a Ritz vector as damage progresses in the 33th member. Here, $\|\cdot\|^2$ denotes the Euclidean norm and $\mathbf{r}^h$ and $\mathbf{r}^d$ denote the Ritz vectors before and after damage occurs, respectively. Figure 4 (b) shows similar quantities for the first five modal vectors, where $\mathbf{v}^h$ and $\mathbf{v}^d$ present the modal vectors before and after stiffness changes, respectively. The shaded portion of the plot indicates that if each component of a modal vector has a 5% of uncertainty level, no measurable change in any modal vector will be apparent unless the stiffness loss exceeds 75%. On the other hand, 10% change of stiffness results in perceivable changes in the second and third Ritz vectors in the presence of a 5% of uncertainty level. As a second example, Figure 5 presents the sensitivity comparison for the stiffness change of the 94th member (a side diagonal in bay six). While the fourth and fifth Ritz vectors are very sensitive to the stiffness change of the 94th member, the change of modal vectors is not apparent until the stiffness loss reaches about 40%. Figure 6 shows that the stiffness change of the face diagonal member 71 does not change the first five modal vectors at all and causes very little change in the Ritz vectors. Similar sensitivity results are observed for all face diagonal members.

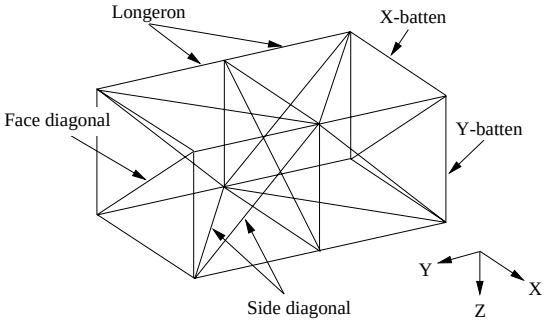

Figure 2. Lacing Patterns of An Eight-Bay Truss Structure

From the sensitivity analyses conducted in this subsection, several observations can be made: (1) In most cases, stiffness changes in the model lead to larger changes in the Ritz vectors than in the modal vectors, (2) face diagonals

(a) Load Pattern 1 (b) Load Pattern 2

Figure 3. Load Patterns Applied to An Eight-Bay Truss Structure

do not cause significant changes to either the Ritz or modal vectors, and (3) in many cases, Ritz and modal vectors are more sensitive to the stiffness losses of side diagonals and longerons than those of battens.

3.2. Damage Detection of An Eight-Bay Truss

This subsection presents the diagnosis results of an eight-bay truss structure conducted under different conditions. First, fourteen damage cases with a single damage location are investigated using different damage threshold values for substructures. Then, six damage cases with either two or three damaged substructures are examined. For all examples, a uniform prior probability is assigned to all hypotheses. Therefore, the determination of the most probable hypothesis in Equation (19) depends only on the error function $J(\hat{\Psi}_{N_s}, \Theta_{H_j}^{max})$. The search space $\Theta_{H_j} < \Omega_{H_j}^*$ in Equation (7) is evaluated at the intersection of grid lines which discretize the search domain with an increment of $\Delta\theta$. For all numerical examples, we use an incremental step $\Delta\theta = 0.1$. The branch-and-bound search in the presented examples follows a depth-first/best-first search strategy.

Ritz vectors are simulated following the generation procedure described in Reference 4 and each Ritz vector is normalized with respect to a reference point. The DOF which has the absolute maximum magnitude in each Ritz vector of the healthy structure, is assigned as a reference point. All the other DOFs are normalized with respect to this reference point. To simulate measurement uncertainties in the estimated Ritz vectors, the estimated Ritz vector set $\hat{\psi}(n)$ in Equation (3) is constructed such that:

$$\hat{\psi}(n) = \psi \ (1 + \frac{\mathcal{N}}{100} \mathcal{R}) \tag{20}$$

where ψ is the exact Ritz vector set obtained from the analytical model, $\mathcal{N}$ is a specified noise level in terms of percentage, and $\mathcal{R}$ is a normally distributed random number with zero mean and a variance of 1.0. This process is repeated N_s times to simulate the N_s data sets.

Excitation is assumed to be a swept sine excitation generated from electrodynamics or hydraulic shakers. All actuators are assumed to generate forces with the same magnitude and phase. The spatial distribution of forces is assumed not to vary with time. Load patterns are selected to maximize the sensitivities of the first five Ritz vectors over all substructures. However, a systematic scheme for the selection of load patterns is not considered here. For all examples, L_{dam} and D_{dam} denote the actual damage locations and the associated damage amount, respectively. $\hat{L}_{dam}$ and $\hat{D}_{dam}$ denote the most probable damage locations and the associated damage amount estimated by the proposed method.

Sensitivity analyses which are similar to Figures 4, 5 and 6, are conducted for load patterns 1 and 2 to define a minimum detectable damage. The *minimum detectable damage* of each substructure is defined as the minimum damage amount which the estimated Ritz vectors from a given load pattern can detect when each component of a Ritz vector is contaminated by a certain level of noise. The minimum detectable damage of each substructure is computed assuming that, because of noise, each component of a Ritz vector is perturbed by 5% of its magnitude.

The branch-and-bound search is conducted including only substructures with damage larger or equal to the pre-assigned minimum detectable damage. The sensitivity analysis in previous subsection show that Ritz vectors have different sensitivities for different substructures. This observation motivates the use of a different threshold for each substructure. The damage thresholds in this subsection are assigned based on the minimum detectable damage. For example, when the minimum detectable damage amount assigned to a substructure is 20%, the corresponding damage threshold is set to 0.8. Noted that when the total removal of a substructure does not cause a perceivable change in Ritz vectors, the substructure is defined as undetectable and excluded from the diagnosis. For example, the 67th member (face diagonal in bay one) is defined as undetectable since the total removal of the member (100%

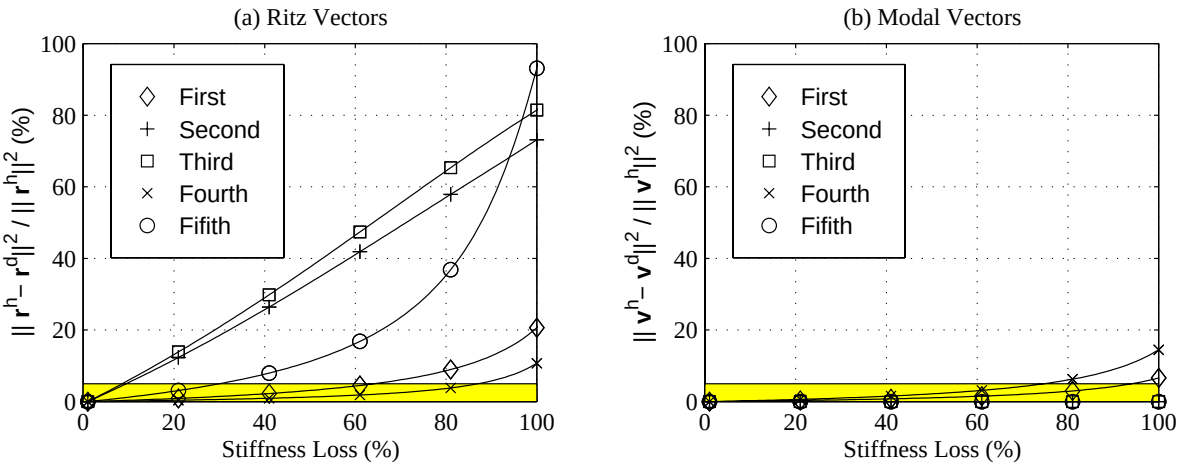

Figure 4. Sensitivity Comparison of Ritz and Modal Vectors for Progressive Damage in Member 33

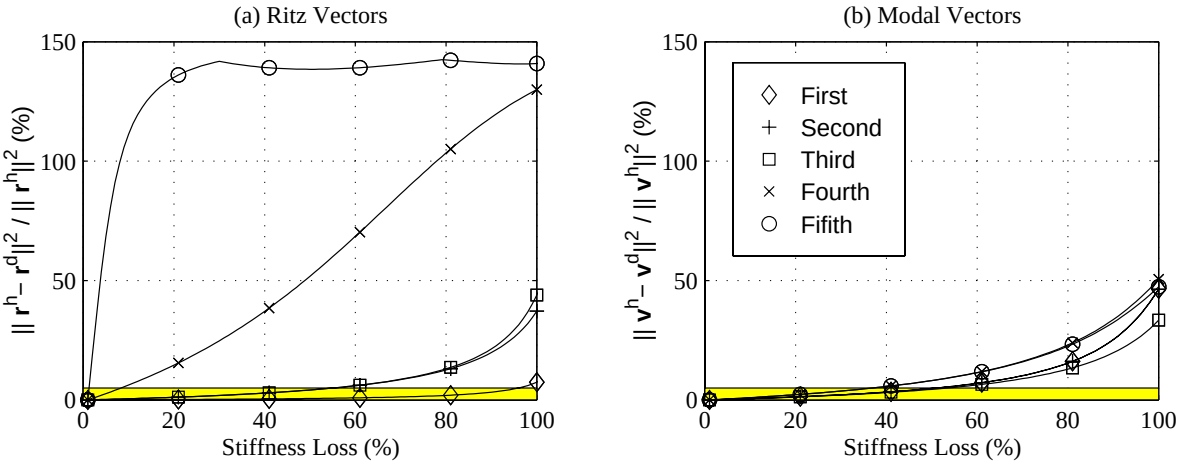

Figure 5. Sensitivity Comparison of Ritz and Modal Vectors for Progressive Damage in Member 94

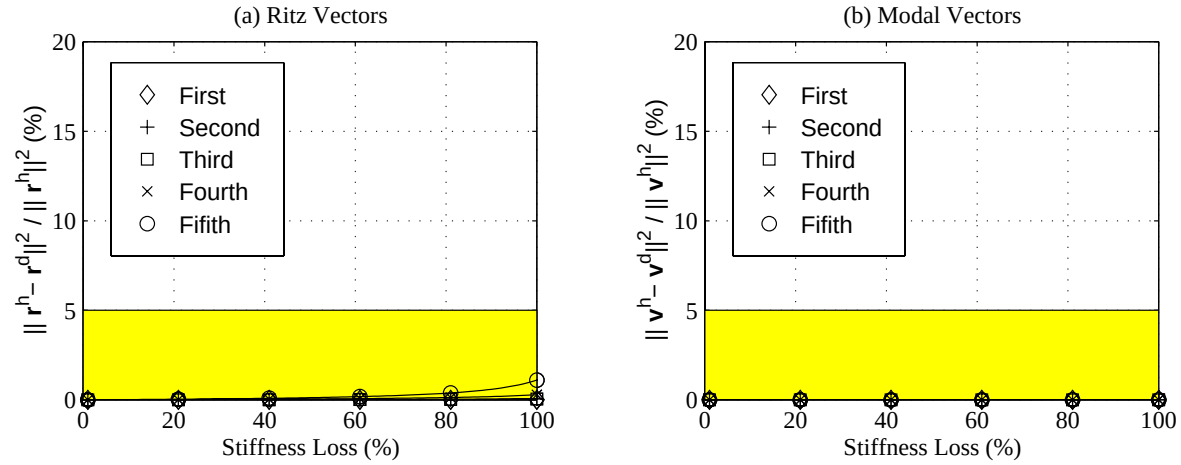

Figure 6. Sensitivity Comparison of Ritz and Modal Vectors for Progressive Damage in Member 71

stiffness loss) does not yield significant changes in Ritz vectors beyond the assumed variation caused by uncertainties. Therefore, the 67th member is excluded from the diagnosis.

Table 1. Diagnoses Using Different Threshold Values

	Actual Damage		Most Prob. Damage		
Case	L_{dam}	D_{dam}	Rank[1]	$\hat{L}_{dam}$	$\hat{D}_{dam}$
A	{46}	{10%}	1/371(350/434)	{46}	{10%}
B	{102}	{10%}	1/552(30/434)	{102}	{10%}
C	{39}	{10%}	1/371(350/434)	{39}	{10%}
D	{97}	{10%}	1/461(55/434)	{97}	{10%}
E	{36}	{10%}	17/95(319/434)	No Damage	
F	{71}	{10%}	-/95(-/95)	No Damage	
G	{33}	{10%}	1/371(372/434)	{33}	{10%}
H	{35}	{10%}	1/461(219/434)	{35}	{10%}
I	{94}	{10%}	1/462(356/434)	{94}	{10%}
J	{28}	{10%}	1/371(382/434)	{28}	{10%}
K	{87}	{10%}	1/371(405/434)	{87}	{10%}
L	{22}	{10%}	1/461(320/434)	{22}	{10%}
M	{17}	{10%}	9/95(428/494)	No Damage	
N	{3}	{10%}	1/461(213/494)	{3}	{10%}

1. The first number is the rank of the actual damage event and the second is the total number of the examined hypotheses. The number in paranthesis is the rank estimaed by the first five modal vectors. "-" denotes that actual damage is not detected.
2. The first five Ritz vectors are estimated from load pattern 2.
3. N_s=1, Noise=5%, and all DOFs are measured.
4. Different damage threshold is assigned to each substructure.

In Table 1, fourteen damage cases with a single damaged substructure are simulated assuming a 10% stiffness loss, a 5% noise level and one data set (N_s=1). Furthermore, all DOFs are assumed to be measured. The damaged substructures used in the examples are shown in Figure 1 by solid lines. For most damage cases, the proposed method identifies the actually damaged substructure as the most probable damage location. The rank of the actual damage event, estimated using the first five modal vectors, is presented in parenthesis of the fourth column of Table 1. The table shows that the first five modal vectors fail to locate the actual damage locations in most cases. In case E, the proposed method indicates that most likely there is no damage. Considering the fact that the damage threshold of the 36th substructure is set to 0.2, the 10% stiffness loss in the 36th substructure is not detectable. The proposed method ranks the 36th substructure as the 17th most probable damage location with 80% damage. Similar results are observed for cases F and M. A sensitivity analysis shows that the stiffness deterioration of the 71th substructure, which is a face diagonal in the 7th bay, does not yield any noticeable changes to the estimated Ritz vectors. Therefore the 71th substructure is precluded from the diagnosis and the proposed method provides a false-negative indication of damage. For case M, the damage threshold of the 17th substructure is set to 0.8. Again the proposed method indicates that most likely there is no damage and ranks the event of 20% damage in the 17th substructure as the 9th most probable damage case.

Next, we focus on the detection of damage in multiple locations. Table 2 presents diagnosis results of six different damage cases. In cases O $\sim$ R, 10% stiffness decrease is simulated in two substructures. Cases S and T introduce 10% stiffness reduction in three substructures. The six damage cases are repeatedly diagnosed under different conditions. In the third column of Table 2, the first five Ritz vectors are generated from load pattern 1 and employed for damage detection. In the fourth column, load pattern 2 is employed instead of load pattern 1. In the last column of the table, a total of ten Ritz vectors are generated from load patterns 1 and 2 (the first five Ritz vectors are generated from each load pattern). For all cases in Table 2, all DOFs are measured and one set of Ritz vectors is simulated assuming a 5% noise level (N_s=1 and Noise=5%).

When the first five Ritz vectors are generated from load pattern 1, the proposed method identifies the actual damage event of cases O, P, Q and T. However, the actual damage locations are not detected for cases R and S.

While the use of load pattern 2 yields the detection of actual damage locations in cases P, Q and R, load pattern 2 fails to identify damage of cases O, S and T. Finally, when a total of ten Ritz vectors are generated from load patterns 1 and 2, the proposed method identifies the actual damage locations for all cases. It is shown that each damage case has different sensitivity to different load patterns and by including more Ritz vectors from different load patterns, diagnosis results can be improved.

Table 2. Diagnoses of An Eight-Bay Truss Structure With Multiple Damage Locations

	Actual Damage		Rank[4]		
Case	L_{dam}	D_{dam}	F1[1]	F2[2]	F1, F2[3]
O	{35,94}	{10%,10%}	1/672	-/371	1/686
P	{39,46}	{10%,10%}	1/483	1/644	1/686
Q	{28,102}	{10%,10%}	1/861	2/914	1/974
R	{39,87}	{10%,10%}	-/672	1/644	1/679
S	{22,35,97}	{10%,10%,10%}	-/672	-/644	1/686
T	{17,35,97}	{10%,10%,10%}	1/577	-/554	1/986

1. The first five Ritz vectors are estimated from load pattern 1.
2. The first five Ritz vectors are estimated from load pattern 2.
3. Load Patterns 1 and 2 are employed and the first five Ritz vectors are estimated from each load pattern (i.e. a total of ten Ritz vectors).
4. The first number is the rank of the actual damage event and the second is the total number of the examined hypotheses. "-" denotes that actual damage is not detected.
5. N_s=1, Noise=5%, all DOFs are measured and the proposed weighting scheme is employed.
6. Different damage threshold value is assigned to each substructure.

3.3. Damage Detection of A Five-Story Three-Dimensional Frame Structure

A five-story three-dimensional frame structure is employed to illustrate the applicability of Ritz vectors to damage detection when differences exist between the baseline structure and the simplified model. The term *baseline structure* is used to refer to a structure from which the experimental Ritz vectors are simulated. In this example, a finite element (FE) model of a five-story frame structure serves as the baseline structure. Figures 7 (a) and (b) show the baseline structure and the simplified model, respectively. While the baseline structure has 6 DOFs at each node (three translational and three rotational DOFs), the simplified model has only 3 DOFs at the mass center of each floor. For the current five-story example, the baseline structure has 120 DOFs and the simplified model has 15 DOFs.

A simplified model, which the proposed method works with, is formed by employing the modeling approach described in Reference 2. The simplified model is constructed assuming that (1) the floor diaphragm is rigid in its own plane and only flexible in the vertical direction, (2) the rotational and vertical DOFs can be condensed out of the dynamic analysis, and (3) the axial deformations of beams and columns are negligible.[6] First, the stiffness matrix of each planar frame is computed and the lateral stiffness matrix of the individual planar frame is determined from the stiffness matrix of each planar frame. Finally, the system stiffness matrix of the three-dimensional structure is obtained by assembling the lateral stiffness matrices of all planar frames. The system mass matrix is diagonalized by lumping the floor mass and the half masses of columns connected to the floor. The moment of inertia of the floor diaphragm is calculated about the vertical axis through the center of mass.

In many vibration tests of building structures, displacements are evaluated at the mass center of the floor diaphragm. Assuming a kinematic constraint that each floor diaphragm is rigid in its own plane, the deformation of the FE model is reconstructed at the mass center of every floor to simulate the real testing conditions. Then, the components of the estimated Ritz vector coincide with those of the simplified model. Loads applied to the baseline structure are also converted to equivalent forces in the simplified model using the displacement transformation matrix which relates the DOFs of the baseline structure to the mass center DOFs of the simplified model. The first six Ritz vectors are estimated from each load pattern. Compared to the previous eight-bay truss example, in which the estimated Ritz vectors are insensitive to most face diagonals and battens, the frame example in this subsection has less redundancy and the estimated Ritz vectors are reasonably sensitive to all substructures. Therefore, the damage threshold is set to 0.9 for every substructure.

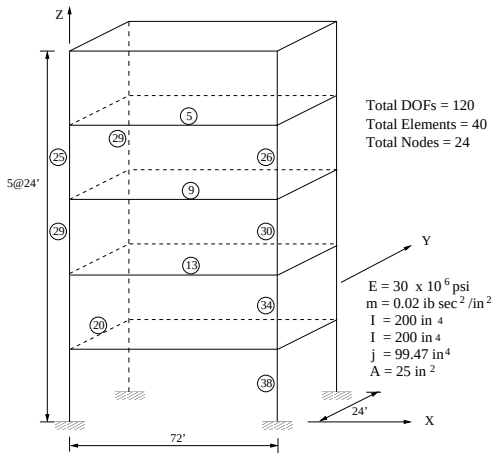

(a) the baseline structure

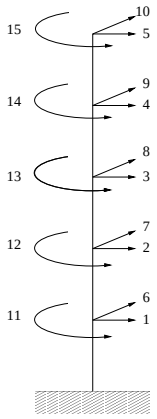

(b) the simplified model

Figure 7. The Baseline Structure and The Simplified Model of A Five-Story Frame Structure

Each beam and column in the baseline structure is modeled as a substructure, and altogether, the system consists of 40 substructures. Since the stiffness matrix of the simplified system is represented as an assembly of the effective stiffness contribution of each substructure (see Reference 2), damage locations can be tracked at the substructure level of the baseline structure. That is, damage locations are identified in the baseline structure, not in the simplified model. Note that using the simplification technique, we are able to reduce the size of the system from 120 DOFs to 15 DOFs without losing significant accuracy. Note that to explicitly consider modeling error into the Bayesian approach, Equation (16) should be modified slightly. This procedure is omitted in this paper but is described in Reference 4.

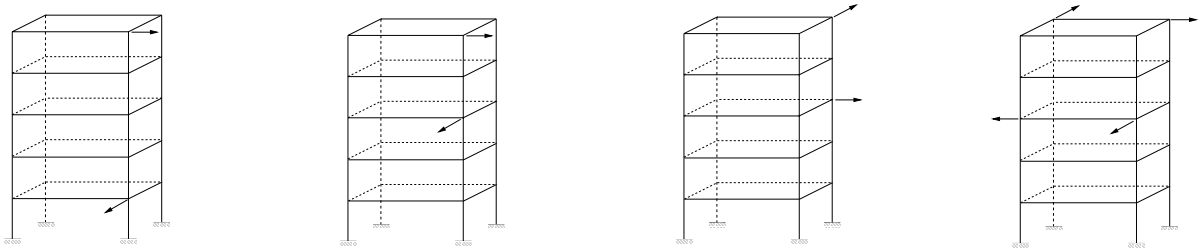

(a) Load Pattern 1 (b) Load Pattern 2 (c) Load Pattern 3 (d) Load Pattern 4

Figure 8. Load Patterns Applied to A Five-Story Frame Structure

Table 3 summarizes the diagnoses of eight different damage cases using four different load patterns and a combination of them. To highlight the effect of modeling error, the effect of measurement noise is neglected in this example. For all damage cases, 10% stiffness decrease is assumed and only one set of Ritz vectors is simulated (N_s=1). Load patterns in the this example are presented in Figure 8. The damaged substructures in Table 3 are shown as circled numbers in Figure 7. For comparison, the results of diagnoses using modal vectors are also presented in the 7th column of Table 3 (denoted as MV in the table). Table 3 shows that a careful selection of load patterns can improve diagnoses of damage and, in general, Ritz vectors provide better diagnoses than modal vectors. For example, by imposing load pattern 1 on the frame structure, the proposed method identifies the actual damage locations in four out of eight cases (cases C, D, E and G). Even for the other four cases (cases A, B, F and H), all the actual damage locations are included in the most probable damage event. Load pattern 2 fails to detect the actual damage event in case H, load pattern 3 does not find the actual damage event of case E, and load pattern 4 ranks the actual damage event as the most probable one only for case G. When all four load patterns are employed simultaneously (the last

Table 3. Diagnoses of A Five-Story Frame Structure Using Four Different Load Patterns

		The rank of the actual damage event[1]					
Case	L_{dam}	F1[2]	F2	F3	F4	MV[3]	All F's[4]
A	{5}	51/266	3/230	3/230	18/255	32/266	1/155
B	{5,9}	8/266	3/266	7/266	15/266	20/266	6/266
C	{13,20}	1/303	2/266	1/375	5/155	100/193	1/230
D	{25,28}	1/193	1/230	1/193	14/230	-/155	2/155
E	{25,30}	1/266	4/266	-/41	2/337	-/41	1/266
F	{9,25}	2/266	2/266	1/266	2/266	-/80	1/302
G	{34,38}	1/266	1/267	2/303	1/303	5/266	1/267
H	{26,29}	7/230	-/41	3/266	2/338	-/41	1/302

1. The first number is the rank of the actual damage event and the second is the total number of the examined hypotheses. "-" denotes that actual damage event is not detected.
2. In F1, F2, F3 and F4, the first six Ritz vectors are estimated from load patterns 1, 2, 3 and 4, respectively.
3. In MV, the first six modal vectors are employed instead of Ritz vectors.
4. Load patterns 1$\sim$ 4 are employed and the first six Ritz vectors are generated from each load.
5. For all cases, D_{dam}=10% and Noise=0.

column of Table 3), the rank of the actual damage event is improved for most damage cases.

In Table 4, the previous damage cases are re-diagnosed (1) using all four load patterns, (2) considering both modeling error and measurement noise, and (3) increasing the number of data sets (N_s) from 1 to 20. Since the use of all the four load patterns provides the best diagnosis in the last examples, all of the load patterns are again employed in this example. To simulate the measurement noise, the analytical Ritz vectors generated from the baseline structure are perturbed with a 5% noise level using Equation (20). Table 4 shows that (1) the diagnoses provided by the proposed method improve as the number of data sets increases, and (2) if load patterns are selected carefully and a large number of data set are available, the proposed method can identify the actual locations and amount of damage even in the presence of measurement noise and modeling error.

Table 4. Diagnoses of A Frame Structure Considering Modeling Error and Measurement Noise

	The Rank of The Actual Damage Event[2]				Most Prob. Damage[3]	
Case[1]	$N_s = 1$	$N_s = 5$	$N_s = 10$	$N_s = 20$	$\hat{L}_{dam}$	$\hat{D}_{dam}$
A	12/230	5/230	2/195	1/155	{5}	{10%}
B	65/303	4/266	2/266	2/266	{4,5,9}	{10%,10%,10%}
C	10/213	4/155	2/193	3/193	{9,20}	{10%,10%}
D	6/155	5/155	3/155	2/155	{28}	{20%}
E	1/303	1/299	1/266	1/303	{25,30}	{10%,10%}
F	2/303	1/266	1/374	1/303	{9,25}	{10%,10%}
G	1/230	1/267	1/267	1/267	{35,38}	{10%,10%}
H	1/337	1/337	1/337	1/266	{25,26}	{10%,10%}

1. The damage cases here are identical to the previous damage cases in Table 3.
2. The first number is the rank of the actual damage case and the second is the total number of the examined hypotheses.
3. $\hat{L}_{dam}$, $\hat{D}_{dam}$ are identified using all the four load patterns and $N_s = 20$

4. CONCLUSION AND DISCUSSION

In this paper, load-dependent Ritz vectors are applied to a Bayesian probabilistic approach to detect the locations and amount of damage. Using Bayes' theorem, the posterior probability of each assumed damage scenario, after observing a set of experimental load-dependent Ritz vectors, are computed. The most probable damage case is searched by comparing the posterior probabilities of different damage scenarios. Then the most likely damaged substructures are

the ones included in the most probable damage scenario (hypothesis) which has the largest posterior probability. A minimum detectable damage of each substructure is defined as the minimum damage amount which the estimated Ritz vectors from a given load pattern can detect when each component of a Ritz vector is contaminated by a certain level of noise. The damage threshold is assigned according to this minimum detectable damage. By assigning a different damage threshold to each substructure, a substructure which causes small changes to the estimated Ritz vectors needs to undergo large stiffness deterioration before the substructure can be detected as damaged and the very insensitive substructures are precluded from a branch-and-bound search. The computational cost of the proposed method is significantly reduced by using a branch-and-bound search scheme and the modeling simplification technique.

Several damage scenarios using an eight-bay truss and a five-story frame structure illustrate the potential use of load-dependent Ritz vectors for damage detection. Diagnosis examples of the truss and frame structures show that, (1) in general, load-dependent Ritz vectors are more sensitive to damage than the corresponding modal vectors, (2) by a careful selection of load patterns, substructures of interest can be made more observable using the Ritz vectors generated from the particular load patterns, (3) if load patterns are selected carefully and a large number of data set are available, the proposed method can identify most of the damage locations, even in the presence of modeling error and measurement noise, and (4) while the extraction of higher modes is difficult, a larger set of Ritz vectors can be estimated by imposing different load patterns.

While this paper has illustrated the potential applicability of load-dependent Ritz vectors to damage detection, many interesting research issues remain. First, even though a procedure to experimentally extract load-dependent Ritz vectors is proposed[1] and the effect of noise on the estimated load-dependent Ritz vectors is studied,[7] real testings should be conducted to validate the experimental procedure. Second, the physical issue of the actuator placement should be addressed to make the extraction of load-dependent Ritz vectors practical. In this paper, we assume that the amplitudes and phases among actuators can be fully controlled and the power requirement to generate the desired excitation forces is not addressed. Third, it is worth while to develop a systematic scheme to find load patterns, which yield better detection of damage in substructures of interest. While the first load-dependent Ritz vector is simply a static deformation of a structure cause by a particular load, a higher load-dependent Ritz vector is orthogonalized with respect to the previous Ritz vectors during the generation procedure, and the relationship between a load pattern and a higher Ritz vector may become obscure. This fact makes the load pattern selection scheme difficult.

ACKNOWLEDGMENTS

This research is partially sponsored by the National Science Foundations under Grant No. CMS-95261-2. The authors wish to express their sincere thanks to Professor David C. Zimmerman of the University of Houston and Dr. Timothy T. Cao of the NASA Johnson Space Center for helpful discussions on the extraction procedure of Ritz vectors and Dr. Scott W. Doebling of the Los Alamos National Laboratory for providing the experimental and analytical data of the eight-bay truss.

REFERENCES

1. T. T. Cao and D. C. Zimmerman, "A procedure to extract Ritz vectors from dynamic testing data," in *The Proceeding of the 15th International Modal Analysis Conference*, pp. 1036–1042, (Orlando, FL), 1997.
2. H. Sohn and K. H. Law, "Bayesian probabilistic approach for structure damage detection," *Earthquake Engineering and Structural Dynamics* **26**, pp. 1259–1281, 1997.
3. J. L. Beck, M. W. Vanik, and L. S. Katafygiotis, "Determination of stiffness changes from modal parameter changes for structural health monitoring," in *The Proceedings of The First World Conference on Structural Control*, (Pasadena, CA), 1994.
4. H. Sohn and K. H. Law, "Application of load-dependent Ritz vectors to Bayesian probabilistic damage detection," *Submitted to Probabilistic Engineering Mechanics* , 1997.
5. T. A.-L. Kashangaki, "Ground vibration tests of a high fidelity truss for varification of on orbit damage location techniques," Tech. Rep. NASA-TM-107626, National Aeronautics and Space Administration, 1992.
6. A. K. Chopra, *Dynamics of Structures*, Prentice-Hall, New Jersey, 1995.
7. D. C. Zimmerman and T. T. Cao, "Effects of noise on measured Ritz vectors," in *The Proceeding of 1997 ASME Design Engineering Technical Conferences*, (Sacramento, CA), 1997.